Multichannel SAR

Pierfrancesco Lombardo
Department of Information Engineering, Electronic and Telecommunications (DIET)
University of Rome "La Sapienza"Via Eudossiana 18, 00184 – Rome
ITALY

lombardo@infocom.uniroma1.it

ABSTRACT

This manuscript describes the potentialities of multichannel SAR (MSAR) in the detection of ground moving targets operating from air- and space-platforms. The knowledge of the moving target provides quite important information of the scenario under observation for both monitoring and intelligence operations. After summarizing the effect of the presence of a moving target inside a SAR image, it is shown how using multiple channels, the targets can be detected even against a strong clutter background. A taxonomy of approaches for MSAR clutter cancellation and target detection is presented. Moreover, a viable processing scheme to detect targets inside High Resolution Wide Swath multichannel SAR images is presented. This exploits a bank of Chirp Scaling Algorithms (CSA), each one matched to a different along track target velocity component.

In addition, two cases of special interest are considered with reference to the sensor characteristics. Since often the number of receiving channels is very limited (especially in space-craft applications), the potentiality to emulate a higher number of spatial channels, by alternating the use of transmit or receive channels among multiple sub-arrays is considered. Moreover, the impact of the observation geometry is considered, which focuses on lately developed techniques for bistatic systems that can be also extended to forward-looking and space-borne applications and is of great interest for future distributed MSAR sytems.

1.0 INTRODUCTION

Nowadays SAR-GMTI (Ground Moving Target Indication) systems are designed in order to meet more and more demanding requirements in terms of GMTI capabilities. Specifically, a SAR-GMTI system is typically asked to detect the moving targets taking benefit of the high resolutions of the SAR sensor. This also requires to maintain high resolution when imaging the moving targets, which requires at the same time to compensate the degradation effects caused by their motion. This can be thought as a first step toward the classification and the recognition of moving targets, thus increasing the overall system surveillance capabilities. In addition, a key feature to increase both surveillance capabilities and situational awareness provided by the SAR-GMTI system is its enhanced potentiality to detect smaller and slower targets. That is, to detect small moving objects inside a SAR image with possible low Radar Cross Section (RCS) and with possibly low Doppler frequencies due to their slow motion.

A detailed analysis of the defects arising when imaging targets moving within the SAR scene is reported in [1]. Here, we briefly recall these effects, in order to properly derive the integrated detection and imaging technique. As it is well known, SAR image focusing is based on the assumption of a stationary scene to be imaged, therefore it is based on the compensation of the relative motion between the SAR platform and the fixed targets on ground. In its simplest modelization this motion is assumed to be rectilinear along the azimuth direction at constant velocity and height, leading to azimuth focusing parameters suitable for conventional SAR processing. However, the same parameters are no more valid when a moving target has to be imaged, since the relative motion is different in this case, [1]. Therefore, to retrieve correct focusing parameters, the relative motion between SAR platform and moving target has to be taken into account.

Referring to the along-track/slant-range plane (x,y) sketched in Fig. 1, this relative motion can be simply expressed as:

$$\begin{cases} x(t_a) = x_0 + \left(V_a + V_t^{at}\right) \cdot t_a + a_x \dfrac{t_a^2}{2} \\ y(t_a) = R_0 + \left(V_t^{ct}\right) \cdot t_a + a_y \dfrac{t_a^2}{2} \end{cases} \tag{1}$$

where x0 represents the azimuthal position of the target at mid-acquisition (we will neglect this term in the following without loss of generality), Va is the SAR platform velocity, Vtat is the target velocity component in along-track direction, ax is the target acceleration in along-track direction, R0 is the target slant range distance at closest approach, Vtct is the target velocity radial component (namely in the cross-track direction), ay is the target radial acceleration, and ta is the slow-time.

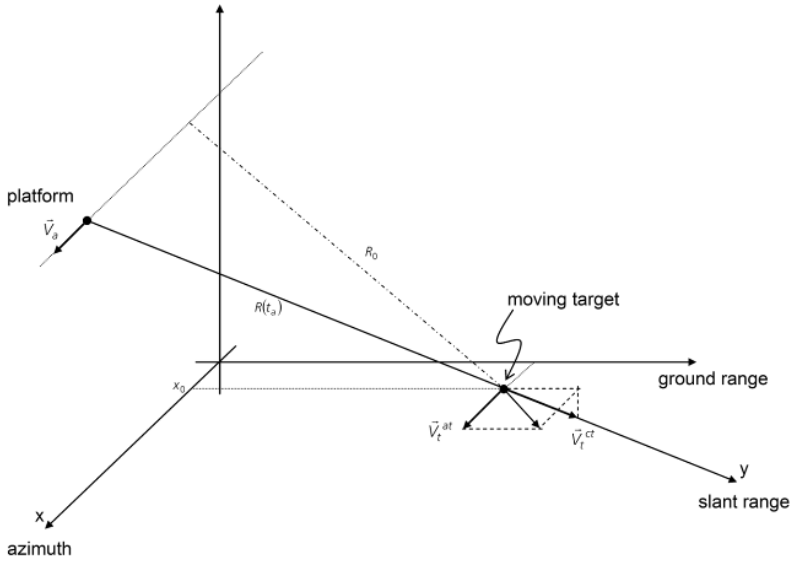

Fig. 1: Acquisition geometry.

Starting from eq. (1), the behavior of the slant-range distances between target and SAR platform (namely R(ta)) can be simply derived, keeping only the second order terms of the Taylor expansion, as:

$$\begin{aligned} R(t_a) &= \sqrt{\left[R_0 + V_t^{ct} \cdot t_a + \frac{a_y}{2} t_a^{\,2}\right]^2 + \left[\left(V_a + V_t^{at}\right) \cdot t_a + \frac{a_x}{2} t_a^{\,2}\right]^2} = \\ &\cong R_0 \left\{1 + \left[\frac{1}{R_0}\left[V_t^{ct} \cdot t_a + \frac{a_y}{2} t_a^{\,2}\right] + \frac{1}{2R_0^2}\left[\left(V_a + V_t^{at}\right) \cdot t_a\right]^2\right]\right\} \end{aligned} \tag{2}$$

Observing eq. (2), it is interesting to notice that the along-track acceleration term (ax) is not present any more. This means that ax only affects higher order terms than the quadratic ones. Therefore, the effects related to along-track acceleration of the movers will not be considered in the following analysis.

On the other hand, eq. (2) states that the second order approximation of the moving target-radar distance contains additional contributions to the terms corresponding to the stationary objects:

- a linear term in t_a, which is present for non-zero radial target velocity components;
- two quadratic terms in t_a^2, one related to radial target acceleration and the other related to along-track target velocity.

The linear term results simply in a Doppler centroid that shifts the focused image of a moving target, thus giving rise to a misplacement of the mover but not affecting the focusing quality. On the other hand, a variation in the quadratic term results in a variation of the azimuth chirp slope, thus leading to smearing effects in the corresponding azimuth focused pulse response, if conventional azimuth processing is performed. Namely, the azimuth processing designed to be a matched filter for the stationary scene, it becomes mismatched for the moving targets. The resulting effects are those related to a mismatch filtering: a degradation of the achievable azimuth resolution as well as a degradation of the moving target signal power obtainable after focusing. These two defects limit the capability to image and to detect a target within a SAR image and, therefore, have to be corrected.

In literature, several solutions have been proposed to provide a SAR system with some GMTI capabilities, each one having a different impact on the SAR system design. The first family of approaches is based on the exploitation of a single-channel SAR system (namely SAR operating with a single receiving antenna beam). The aim is mainly to provide a SAR system with some GMTI capabilities keeping limited the hardware, the amount of data and the cost. This is not expected to provide a strong target detection capability (i.e. no small RCS and/or small velocity targets detection). The simplest approach is to perform the moving target detection working in the Doppler domain only, namely by synthesizing a filter with a notch centered in the Doppler centroid of the stationary scene, so that returns from the stationary background are cancelled. The main drawback is that only exo-clutter moving targets can be detected, that is only targets fast enough to produce echoes with Doppler frequencies out of the clutter Doppler bandwidth. Another low-cost approach is to divide the overall synthetic aperture in several sub-apertures, focus each sub-aperture independentely at reduced azimuth resolution, and detect moving targets as “changes” in the sequence of low-resolution SAR images, [2]. It is clear that single-channel SAR-GMTI becomes an interesting solution when moving targets characterized by strong echoes are considered. In this case, their detection against stationary background is not an issue, and one might aim at compensating target motion defects [1] in order to provide correct focusing,[3], [4].

While this is effective for the detection of targets with relatively high signal to disturbance power ratio, it is well known that the capability of single-channel SAR to detect targets in sub-clutter visibility condition is limited. In contrast, multi-channel SAR systems (namely SAR equipped with multiple receiving antennas or antenna fraction connected to independent receiving channels) can provide detection capability for slower and lower RCS targets, by mean of a significant disturbance cancellation capability. In this case, the availability of multiple parallel receiving channels gives additional Degrees Of Freedom (DOFs) to suppress returns from the stationary background (i.e. ground clutter), thus making easier the detection of movers. The most attractive solutions for multi-channel SAR-GMTI are based on an adaptive cancellation of the clutter echoes, also referred to as Space Time Adaptive Processing (STAP) techniques for SAR, [5], [6], [7]. A commonly used configuration includes the parallel receiving channels connected to different antenna sub-apertures aligned in the along-track direction. Spatial samples corresponding to different Pulse Repetition Intervals (PRI) are combined coherently with proper complex weights in a space-time filter that cancels the echo backscattered from the ground making visible the signals corresponding to moving targets. Such a two-dimensional filtering leads to much higher moving target detection performance w.r.t. a one-dimensional filtering (either space-only or time-only filtering). The optimum way to coherently combine space-time samples can be derived analytically,[5]. This optimum weights derivation ensures the maximization of the Signal to Clutter plus Noise Ratio (SCNR) after filtering. In practical cases, some sub-optimal STAP configurations have been derived to limit the overall number of spatial and temporal DOFs, aiming at keeping limited the overall computational burden.

2.0 MULTICHANNEL SAR FOR GMTI

As shown in Fig. 1, ground moving targets observed by SAR are reported misplaced and potentially defocused inside the image, as a consequence of their motion. This is because the SAR focusing exploits the one-to-one relationship between Doppler frequency and angle of arrival that applies to stationary objects. The presence of the target own velocity components modifies this relationship. It is therefore of high interest for surveillance and intelligence purposes to: (i) detect the moving targets inside SAR images, (ii) refocus them, so as to allow appropriate target recognition.

The use of multiple receiving channels with an along track displacement provides an angular discrimination capability that can allow the removal of the ambiguity between Doppler frequency and angle of arrival, and the identification of the targets that are not stationary. For high RCS targets that compete against a low clutter background the target detection can be obtained by comparing the images taken by the multiple channels. In contrast, it is impossible to detect low RCS moving targets competing against a strong clutter background, unless a preliminary cancellation filter has been applied to reduce the stationary clutter returns.

To this purpose, we consider the problem of clutter cancellation and slowly moving target detection in modern radar systems equipped with digital beamforming. These systems use STAP techniques to cancel the radar clutter and detect also ground slowly moving targets, that have a Doppler frequency well inside the clutter spectrum. The performance of such systems is limited by the following:

a) the sensor characteristics (among which: number of pulses in the coherent processing time, pulse repetition frequency (PRF), number of receiving channels, antenna size and pattern);

b) the severity of the clutter scenario (described by the spread of its internal motion);

c) the observation geometry (monostatic/bistatic, side/forward-looking, air/space-borne).

After briefly recalling the basics of multi-channel radar detection of moving targets from a moving platform, this text describes a few advances.

2.1 Model and interpretation for multichannel SAR echoes

Reference is made to a side-looking radar system with N spatial channels obtained transmitting with the whole antenna array and receiving with N antenna sub-apertures displaced in the along-track direction. Each of these sub-arrays receives M echoes from a transmitted train of M coherent pulses with a Pulse Repetition Time (PRT) of T s. Let xm,i be the radar echo at the i-th spatial channel (i=1, …, N) in response to the m-th pulse (m=1, …, M). The NM echoes represent a space-time snapshot and can be arranged into the NM-dimensional column vector $\mathbf{x} = [\mathbf{x}_1^H \ \dots \mathbf{x}_M^H]^H$, being xm the column vector of the N echoes received at the m-th pulse. In the presence of a target with Doppler frequency F (normalized to PRF=1/PRT), DOA (Direction of Arrival) φ and complex amplitude A, the snapshot can be written as $\mathbf{x} = A\mathbf{s}(F,\varphi) + \mathbf{d}$, where d is the disturbance (clutter+noise) component and s is a NM×1 vector called the target space-time steering vector. It may be expressed as $\mathbf{s} = \mathbf{s}^{(t)}(F) \otimes \mathbf{s}^{(s)}(\varphi)$ where $\mathbf{s}^{(t)}(F) = \left[1 \ e^{-j2\pi F} \dots e^{-j2\pi F(M-1)}\right]^H$ is a M×1 temporal steering vector and $\mathbf{s}^{(s)}(\varphi_t) = \left[1 \ e^{-j\Delta(\varphi_t)} \dots e^{-j\Delta(\varphi_t)(N-1)}\right]^H$ is a N×1 spatial steering vector. $\Delta(\varphi)=2\pi(d/\lambda)\cos(\theta)\cos(\varphi)$ is the inter-channel phase shift, which is a function of DOA φ and depends on antenna sub-aperture spacing d, radar wavelength λ and depression angle θ, [5]. Under Gaussian assumption for the statistic of the space-time snapshot x, its Probability Density Function (PDF) is:

$$p(\mathbf{x}) = \frac{1}{\pi^{NM}|\mathbf{Q}|}\exp\left\{-[\mathbf{x}-A\mathbf{s}]^H \mathbf{Q}^{-1}[\mathbf{x}-A\mathbf{s}]\right\} \quad (3)$$

where Q=E{ddH} is the NM×NM space-time covariance matrix of the disturbance, [8]. The mean vector, E{x}=As, is assumed to be known, aside for the complex amplitude, A, which is identically zero under hypothesis H0 (absence of target) and has an unknown value under hypothesis H1 (presence of target). Under these hypotheses, the well-known Optimum Adaptive Processor (OAP) is given by the NM-dimensional weight vector $\mathbf{w} = \mathbf{Q}^{-1}\mathbf{s}$.

To evaluate the performance, we consider the Signal-to Clutter-plus-Noise Ratio (SCNRout) at the output of the adaptive filter as a function of the normalized Doppler frequency F. Fig. 2 shows the SCNRout obtained with the OAP for the case of a radar operating with a linear antenna array of 120 radiating elements, beam pointing at φL=90°, M=64 PRIs. We assume a Gaussian temporal clutter correlation, with reflectivity σ_0=-15 dB and a target RCS of 15dB. We consider the two different cases obtained by transmitting with the whole antenna aperture (Standard Transmission – STTX) and respectively:

- N=1 receiving channel (curve with symbol "×"), namely receiving with the whole antenna aperture;

- N=2 receiving channels (curve with symbol "∇"), namely receiving with two adjacent sub-arrays of 60 radiating elements each.

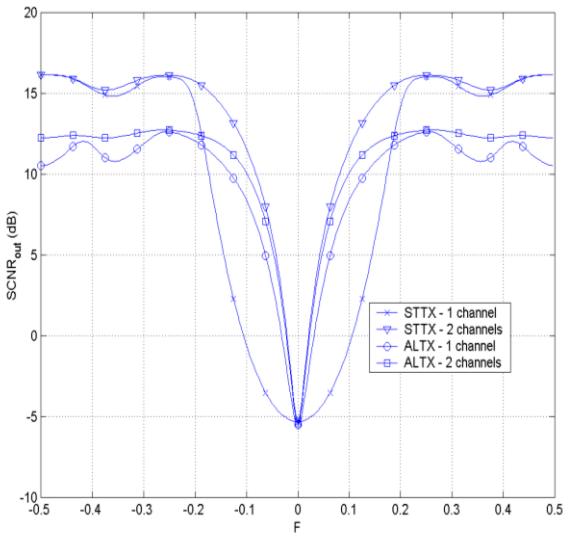

Fig.2 –SCNRout curves for N=1,:STTX and ALTX.

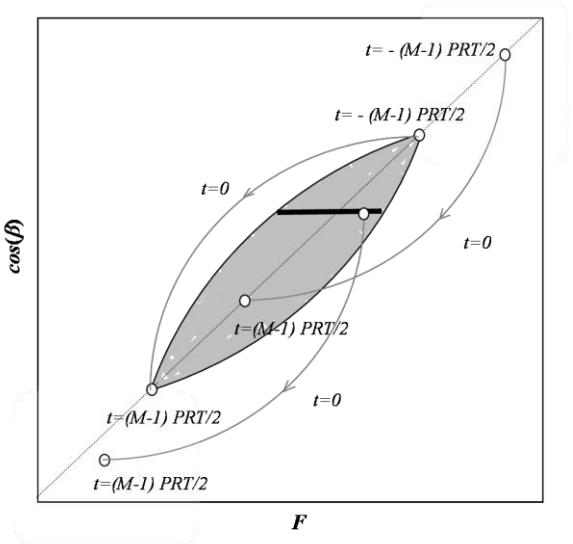

Fig. 3 - Frequency-Angle plane.

Obviously, using a STTX approach with a single receiving channel allows an adaptive filtering, that involves only the temporal dimension. In consequence, for STTX with N=1 the spread of the clutter spectrum due to the platform motion yields a filter notch that depends on the antenna beam-width. For N≥2 an angular discrimination capability is available, which allows a proper bi-dimensional filtering in the Frequency-Angle plane of Fig. 3 (with cosβ=sinφ), which is the typical representation plane for the MTI radar STAP, [5]. Specifically the optimum filter can be interpreted as the cascade of a notch filter on the clutter diagonal in this plane, followed by a target enhancement filter, that aims at performing a coherent integration for target searched at a specific Doppler frequency-DOA position in the plane. As expected, increasing the number of spatial channels, does not give any advantage far away from the clutter notch, where the performance is only limited by the available signal power and the thermal noise level. In contrast, the clutter notch becomes

narrower as the number of receiving channels increases, which is paid in terms of complexity of the radar hardware, since a larger number of parallel receiving channels must be implemented, and computational load, since the dimensionality of the data to be filtered is increased.

The Frequency-Angle plane in Fig. 3 is the preferred representation for the echoes in multichannel systems. A short observation time is assumed, so that Doppler frequency and DOA of the single scatterer are constant and the array is used to exploit the scatterers angle. In contrast, when the observation time is long, both DOA and Doppler frequency of the clutter echo from the single surface scatterer depend on time. This can't be represented in the plane above, where the echo from each clutter patch moves in time along a line with constant slope (arrows in Fig. 3). The scatterers that quit the antenna beam are replaced by the new ones entered, and the same 2D Power Spectral Density is observed. The Time-Frequency plane in Fig. 4 is the preferred representation for single channel SAR, where a long observation time is considered. It allows the representation of the time varying Doppler frequency but it doesn't contain any angular information. The Doppler frequency of any scatterer in this plane is ambiguous: it refers to a combination of cross-track velocity and angular position.

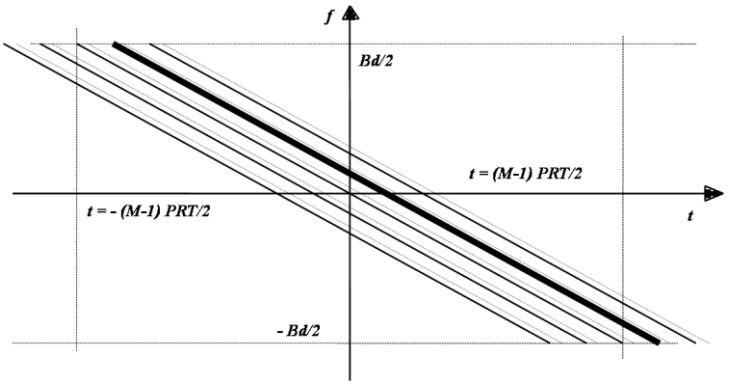

Fig. 4 - Frequency-time plane: typical of SAR.

The M-SAR allows Doppler and angular information to be decoupled by means of along-track interferometric processing. To fully interpret the MSAR echoes, a 3D Angle-Time-Frequency space, in Fig. 5 is required, which allows both Doppler frequency and DOA to be represented as functions of time, [6], [8]. Its integration over time collapses it back into the Frequency-Angle plane, while its integration over angle collapses it into the Time-Frequency plane. In this space the relative motion of the stationary scatterer echoes in the Doppler-angle limits of the antenna beam are correctly represented (_._). The generic target echo (_.._), with velocity components different from the background can also be effectively represented and discriminated from the clutter echoes.

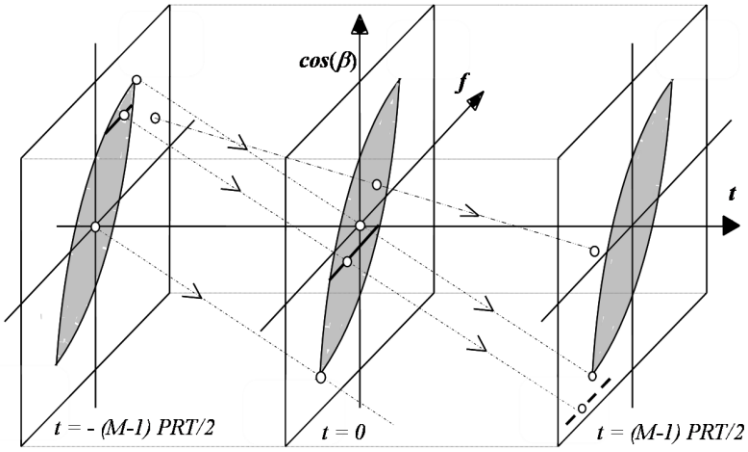

Fig. 5 - Space-frequency-time volume: typical of MSAR.

2.2 A taxonomy of multichannel SAR techniques

Many processing schemes have been proposed in the past years to detect moving targets using the echoes received during the long sequence of M PRI by SAR with N antennas. They follow different approaches to deal with the three parameters: along track velocity (Doppler rate), cross track velocity (Doppler), angle of arrival (DOA), [6]. A first approach is to use the multiple antennas to emulate a "non-moving" platform and look for echoes from moving reflectors using the pixel phases. This generates two techniques:

A) Along Track Interferometry SAR (ATI-SAR). A SAR image is generated for each of the two displaced antennas. After compensating the phase due to the time delay between the two images of a stationary scene, any residual phase difference between the images reveals a moving target, [9].

B) Velocity SAR (VSAR). N complex SAR images are produced with preserved phase. The "velocity planes" are obtained by Fourier transformation along the N receivers and are phase shifted by an amount proportional to their velocity to correct the motion induced azimuth displacement. All planes are summed to yield the final VSAR image, [10]. This is clearly not designed to suppress clutter, but only to focus the moving target.

A second approach is to use the multiple antennas to emulate a "non-moving" platform and cancel the echoes from the stationary background to maintain only moving target echoes. This idea generates the:

C) Displaced Phase Centre Antenna (DPCA) for SAR. By selecting a PRF in relation to both platform speed and displacement of the two antennas, their 2-way phase centres are occupy the same positions in subsequent PRIs. Thus, stationary clutter is seen at two different time instants from the same radar location and it can be cancelled by subtracting the corresponding echoes, whereas the moving targets do not cancel due to the Doppler-induced phase shift. The simplicity of this scheme is paid by very strong constrains on antenna, PRF and speed. An extension of this approach, which removes such constraints is to use STAP instead of DPCA to cancel clutter.

The ideal detection scheme, which yields theoretically the best performance, is given by the

D) optimum filter with very long integration time: Filter characterised by a target steering vector with Doppler frequency and DOA that are not constant during CPI. However it has the full computational complexity due to the 3D filter bank (Doppler rate, Doppler, DOA). In special cases this optimal solution can be derived and interpreted, [11]. In such cases it becomes coincident with scheme E or G below.

Moreover, a FIR (Finite Impulse Response) filter approximation of the optimum filter leads to:

E) STAP filtering + coherent integration for SAR processing. Use first a STAP cancellation filter, that performs the clutter cancellation and collapses the N channels into a single ideally "clutter free" channel, [11],[12],[13]. A 2D filter bank follows (Doppler rate, Doppler) to detect the target. This scheme has reasonable computational cost (see Fig. 6a) and reasonable performance.

Finally, two low cost implementations can be obtained by using optimum filters after a preliminary non-adaptive coherent integration and a data reduction applied respectively in in the Doppler-DOA and in the Doppler dimension:

F) Joint Domain Localised (JDL) for M-SAR. First a time-varying transformation is applied to the space-time data to compensate for the time-varying Doppler frequency of the clutter echoes. Therefore, a large reduction of degrees of freedom is performed in the Doppler-DOA plane, after 2D FFT. This is followed by an adaptive filter applied in the reduced domain, [14].

G) Processing in the frequency domain. First apply a Fourier transform to the temporal sequence of samples received by each of the N receivers. Moderate synthetic aperture length is sufficient to make negligible the correlations between frequency channels. This is the key to use projection methods with the advantage that the clutter is cancelled perfectly without sensitivity to its amplitude variations, [15]. The computational load is affordable for few spatial channels. See Fig. 6b.

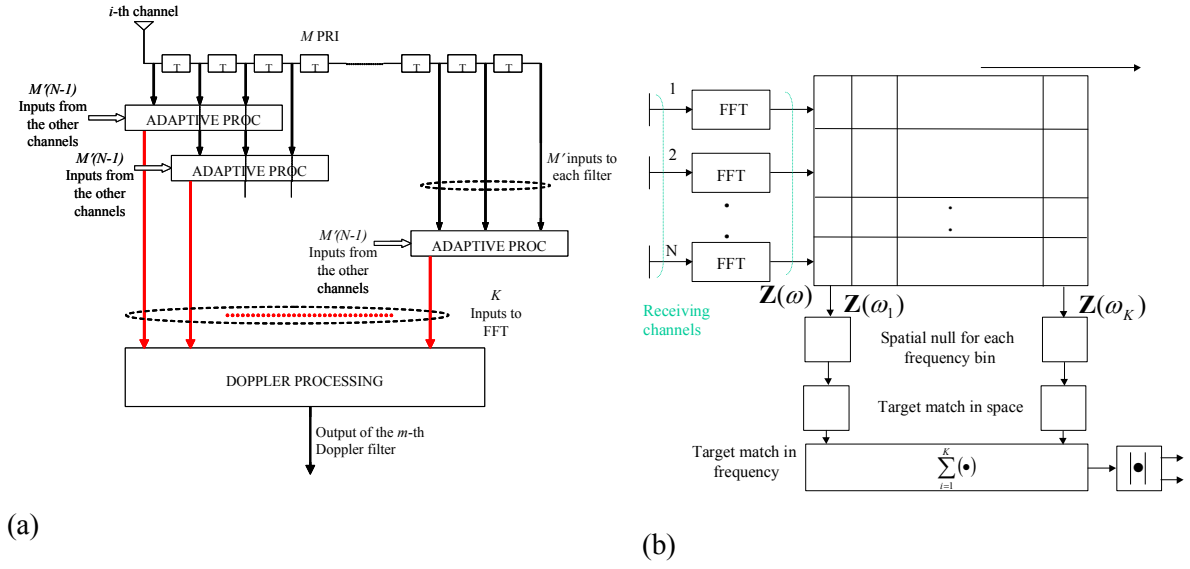

Fig. 6 – Sketch of (a) STAP+SAR processing; (b) frequency domain processing.

3.0 GMTI IN HIGH RESOLUTION WIDE SWATH SAR

From the analysis of eq. (2), it is interesting to notice that the motion of the target with respect to stationary ground does not affect only the azimuth processing, but also the Range Cell Migration (RCM). In particular, while a radial target velocity component gives rise to the range walk effect, the target movement in the along-track direction affects the range curvature (that is, the quadratic term of the RCM). The presence of the RCM is especially important in the case of High Resolution and Wide Swath, where the high resolution implies a strong cell migration, whereas the wide swath implies a change in the RCM trajectory for the different points inside the image.

Moreover, observing eq. (2), it is clear that along-track velocity Vtat and radial acceleration ay both affect the quadratic term of R(ta), thus giving rise to undistinguishable effects. In the following analysis, for the sake of simplicity, we will always refer only to variations of the quadratic term of R(ta) due to the presence of along-track velocity component (assuming negligible the radial acceleration ay, or better to be non discriminable from the along-track velocity). This adds to the standard variation of the quadratic term that is already present in the high resolution wide swath images of a stationary scene. Therefore, the appropriate compensation of the quadratic phase term for the moving targets has to cope with both effects.

The processing technique for the detection of moving targets in Wide Swath High Resolution SAR images requires to include all the compensations that are considered by the advanced SAR focusing techniques well known for the fixed scene. Among these compensations the following need to be mentioned: (i) range migration compensation with migration path possibly changing from near field to far field and with target velocity components; (ii) azimuth focusing parameters changing from near field to far field and with target velocity components.

An appropriate compensation technique is first considered in sub-section 3.1 for a single channel SAR image and then extended the multichannel case subsection 3.2. The result is a complete scheme including all these compensations, together with the STAP clutter cancellation

3.1 Single channel SAR moving target detection

It is interesting to notice that the difference in range and phase compensation required to focus the moving targets, compared to those used for the fixed scene, can provide a certain degree of clutter rejection, so that it is even possible to attempt the detection of high RCS targets inside a single channel image. Assuming that in the general case no a priori information regarding the target motion is available, a complex focusing algorithm is presented below, which takes into account a possible along-track movement of the targets. A bank of several azimuth compression filters is synthesized, each one matched to a different relative along-track velocity between SAR sensor and moving target, following a similar approach to [16].

Despite a high number of filters is required, which directly increases the computational cost, it is possible to implement the bank of filters that includes all the required compensations by exploiting the efficient Chirp Scaling Algorithm (CSA), [17], thus largely reducing the computations. Such a bank of CSA-based focusing filters is able to largely recover SCNR degradation due to focusing mismatch, thus increasing moving target detection capabilities even in a single-channel SAR system, [18]. The processing chain required by the Single Channel - Bank of Chirp Scaling Algorithms (SC-BCSA) technique is sketched in Fig. 7.

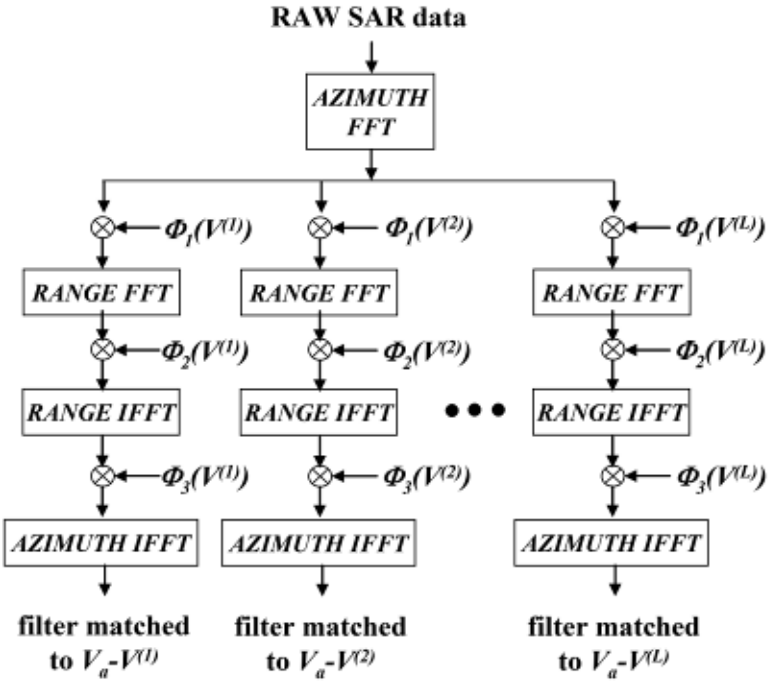

Figure 7: Processing chain for the SC-BCSA technique.

The chain comprises a number L of branches being each branch a CSA with parameters (the Φ_1, Φ_2, and Φ_3 phase multiplication terms, [17]) matched to a different possible target velocity component in the along-track (a.t.) direction. This means that in each CSA branch within the bank, the a.t. sensor velocity Va has to be replaced with the relative a.t. velocity between sensor and potential target (V(i)). Consequently, all the processing steps which depends on Va for each of the L branches can be applied in parallel with the appropriate values. Specifically, the application of Φ_1 and Φ_2 with the target along track velocity leads to a correct equalization and correction of the range curvature terms corresponding to the along-track target motion, whereas the application of Φ_3 is responsible for a correct azimuth compression step.

As apparent, the use of a bank of CSA schemes has the important advantage to take care jointly of both focusing filters and RCM compensation. Moreover, the CSA has been selected because of its computational efficiency, namely no interpolations are required like in the case of Range-Doppler or Range Migration Algorithm. Moreover its first operation is an azimuth FFT: this is an attractive characteristic having in mind to extend it to operate for a multi channel SAR system, to integrate the bank of filters together with a post-Doppler STAP approach. This will be analyzed in the following subsection.

For a time observation interval T, the number of branches (CSA filters) L needed to maintain peak losses in the azimuth pulse response within 3 dB is given by $L = (\mu_{MAX} - \mu_{MIN}) / \delta\mu$ where $\delta\mu = 1.8/T^2$ is the chirp rate resolution, [16], and the maximum and minimum values of the quadratic term to be considered is obtained from

$$\mu_{MAX/MIN} = \frac{2\left(V_a + V_{t,MAX/MIN}^{at}\right)^2}{\lambda R_0} \tag{4}$$

being Vatt,MAX/MIN the maximum and minimum along track target velocity components.

Each mover will be differently focused in the L images at the output of the L branches, showing a maximum peak level in the image obtained by using the a.t. velocity value that better approximates the relative actual a.t. velocity between target and sensor. A proper threshold (as for example obtained via a 2D Cell Average, CA, CFAR) can then be applied to each output image to detect the movers.

To show the effectiveness of the SC-BCSA technique, an emulated SAR dataset has been derived in [18] starting from a focused SAREX-92 image of the Tapajos rain forest [19][20] with 6 meters resolution, Fig. 8.

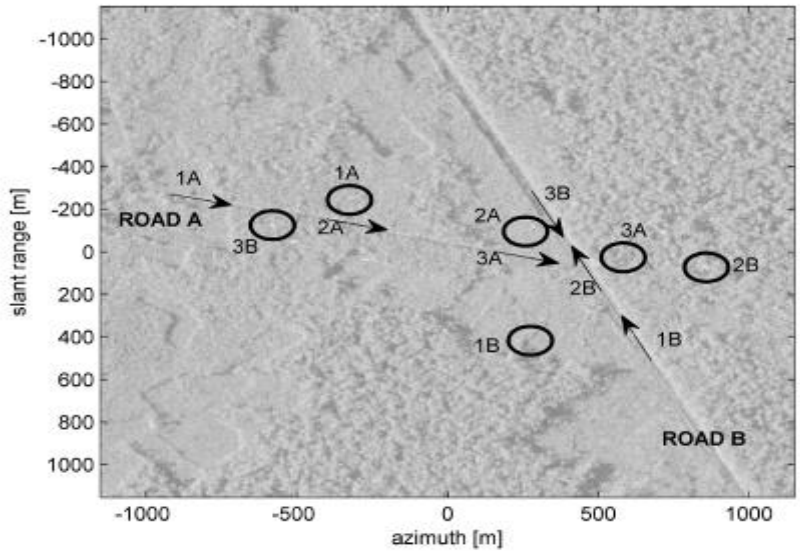

Fig. 8: SAREX image with synthetic movers.

To use such an input image for demonstration purposes, an inverse focus processing has been applied to obtain the raw single-channel SAR data of stationary background. Such a raw dataset of the stationary background has been added to raw returns from synthetic targets moving along roads A and B (see Fig. 8).

Tab. 1: Moving targets velocities.

Target	Velocity [m/s]	Radial component [m/s]	A.t. component [m/s]
1A	22	5.37	21.28
2A	10	2.44	9.67
3A	5	1.22	4.83
1B	-10	-8.78	-4.13
2B	-22	-19.33	-9.10
3B	7	6.16	2.89

Movers inserted in the image (see Tab. 1) are represented by arrows indicating their true position and corresponding motion, while circles indicate the displaced position of their corresponding echo in the focused image due to their radial velocity. The considered scenario leads to a dwell time of about 1 second for the targets. The maximum target velocity of 22 m/s (absolute value) has been selected, resulting in L=11 branches in the bank of CSA.

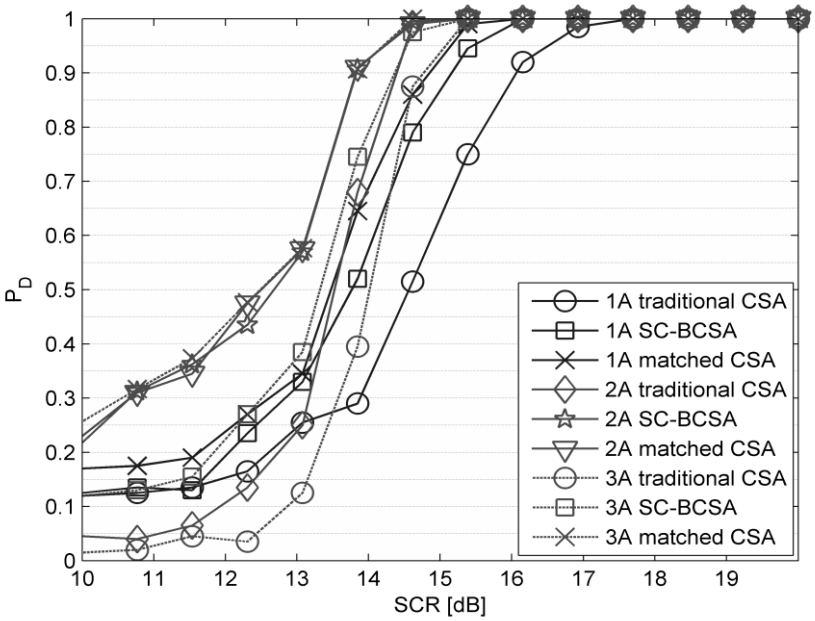

Fig. 9: PD vs. SCR: bank of CSA – road A.

The first advantage related to the use of the SC-BCSA technique is the moving target detection improvement. To show this, a Monte Carlo simulation with 300 trials has been conducted for increasing SCR and different speckle realizations. Moving targets are detected via a 2D CA-CFAR (Pfa set to 10-4) applied to the output image from each branch of the bank. Detection performance is expressed in terms of PD versus SCR and reported in Fig. 9 for the targets on road A.

Detection performance obtained by applying conventional focusing (the CSA matched to the stationary background) is compared with the performance achievable by the SC-BCSA technique (only the branch that gives the higher output power is considered), and with by a matched focusing (the CSA based focusing matched to the actual a.t. velocity of the target). As expected, targets characterized by a higher a.t. velocity component are those that experience a higher detection improvement by implementing the proposed SC-BCSA technique w.r.t. the traditional CSA processing. Moreover, it is worth to notice that the detection performance of the bank of CSA is comparable w.r.t. the matched CSA, thus ensuring that a sufficient number of focusing filters has been considered.

The mis-match reduction in moving targets focusing causes also an improvement in the achievable azimuth resolution. To show this, the focusing of the movers has been reported for target 1A in Fig. 10. The azimuth main cut of the target response obtained after the traditional CSA focus is compared with the corresponding responses obtained after the bank of CSA and after the matched CSA. Moreover, the pulse response obtained after a Matched Filtering (MF), including a range walk correction step, is reported for a theoretical comparison. By using the SC-BCSA technique the azimuth response main lobe becomes clearly visible, differently from the case of the traditional CSA. Moreover, the matched CSA case does not yield to substantial differences w.r.t the bank of CSA. By comparing the bank of CSA and the MF responses, it is possible to appreciate both a reduction in the response peak, and a degradation in the azimuth resolution. This latter effect is due to the reduced time the target remains in the same resolution cell.

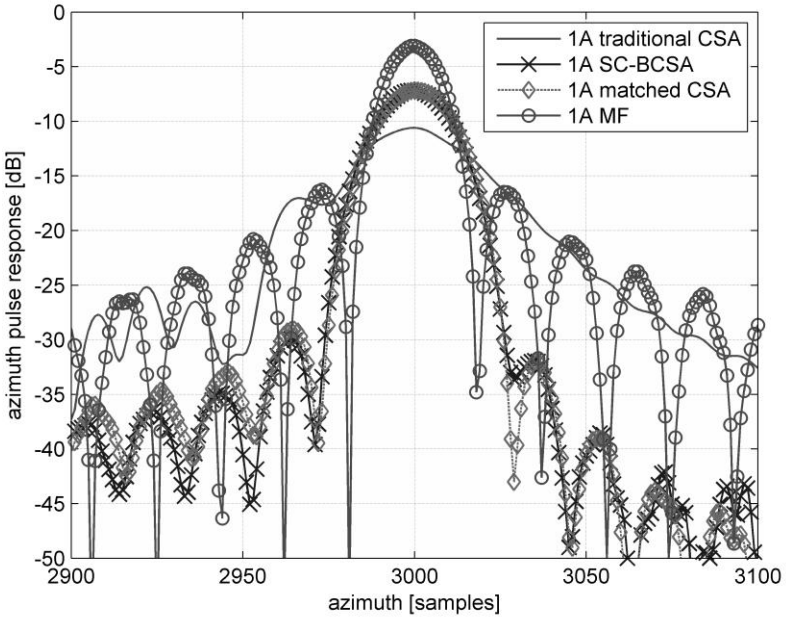

Fig. 10: Comparison of azimuth pulse responses – target 1A.

It is worth noting that the proposed technique takes into account only an a.t. target velocity component, while no processing is considered to compensate range walk effects due to cross-track (c.t.) target motion. A range walk correction step can be performed before the bank to avoid the degradation due to uncompensated cross-track motion.

3.2 Multichannel SAR moving target detection

The SC-BCSA presented above is able to recover imaging capability for the moving targets present in the observed scene. However the SCNR recovery provided by the single channel technique can be not sufficient to ensure a reliable moving target detection especially if sub-clutter moving target detection capabilities are required. In such conditions, a M-SAR system has to be considered and the bank of CSA has to be combined with a clutter cancellation step, such as a STAP technique.

This approach can be nicely implemented together with the Multichannel SAR approach G, [15]. An azimuth Fourier transform is performed independently for each parallel receiving channel prior than STAP filtering. This post-Doppler approach to STAP guarantees, for the SAR case, a theoretical decoupling of different Doppler bins, [21]. As a consequence, a clutter cancellation can be performed separately for each Doppler bin using only the spatial DOFs (which are usually a limited number in a M-SAR system). This results in small dimensions of the covariance matrices to be estimated and inverted, thus maintaining limited the computational burden. The results is a complete scheme that integrates the single-bin post-Doppler clutter cancellation approach together with the bank of CSA-based moving target focusing scheme presented for the single-channel SAR, [18]. The integrated scheme capitalizes on the fact that both the selected cancellation and focusing approaches start with a FFT in the slow-time domain, to provide an efficient implementation that ensures an overall limited computational burden.

Specifically, being the correlation between adjacent Doppler bins very limited, it will be neglected in the following analysis, thus leading to a clutter cancellation performed Doppler bin per Doppler bin using only spatial DOFs (i.e. factored post-Doppler STAP, [22]).

The signal model used for the derivation of the adaptive STAP filter weights is the following. Let us indicate with xk,n the M×1 received data vector from k-th range bin and n-th receiving channel obtained after Discrete Fourier Transform in the azimuth domain (where k=1,...,K and n=1,...,N). Indicating with k the range bin of interest (that is, the range bin where the presence of the target has to be tested), the Fourier transformed data from all N receiving channels corresponding to the m-th Doppler bin is expressed as

$$\mathbf{y}_{k,m} = \begin{bmatrix} x_{k,1}(m) \\ \dots \\ x_{k,N}(m) \end{bmatrix} \tag{5}$$

yk,m is a spatial-only data vector with dimensions N×1 that contains a potential contribution from a moving target, and a Gaussian interference contribution having second order statistics described by N×N covariance matrix Rk,m. Under the assumption of local stationarity of the interference over range, the unknown interference covariance matrix Rk,m can be replaced with its maximum likelihood estimate obtained from adjacent range gates

$$\hat{\mathbf{R}}_{k,m} = \frac{1}{P}\sum_{p} \mathbf{y}_{p,m}^{H} \cdot \mathbf{y}_{p,m} \tag{6}$$

where p indicates secondary range gates adjacent to the range gate under test k. To prevent potential target sidelobes to be present in the secondary data, the pair of range gates right next to the gate under test are taken as guard gates and are usually excluded from covariance matrix estimation. After invertion of the estimated covariance matrix, the N×1 adaptive weight vector for k-th range gate and m-th Doppler bin can be derived

$$\mathbf{w}_{k,m} = \hat{\mathbf{R}}_{k,m}^{-1} \cdot \mathbf{s}_{m}, \tag{7}$$

sm being a N×1 secondary beamformer indicating the spatial desired target steering vector. The corresponding clutter-free sample rk,m is then obtained as:

$$r_{k,m} = \mathbf{w}_{k,m}^{H} \cdot \mathbf{y}_{k,m} \tag{8}$$

The adaptive processing is then iterated for all range and Doppler bins. A sketch of the resulting post-Doppler STAP technique is reported in Fig. 11 for the sample case of three parallel receiving channels, [18].

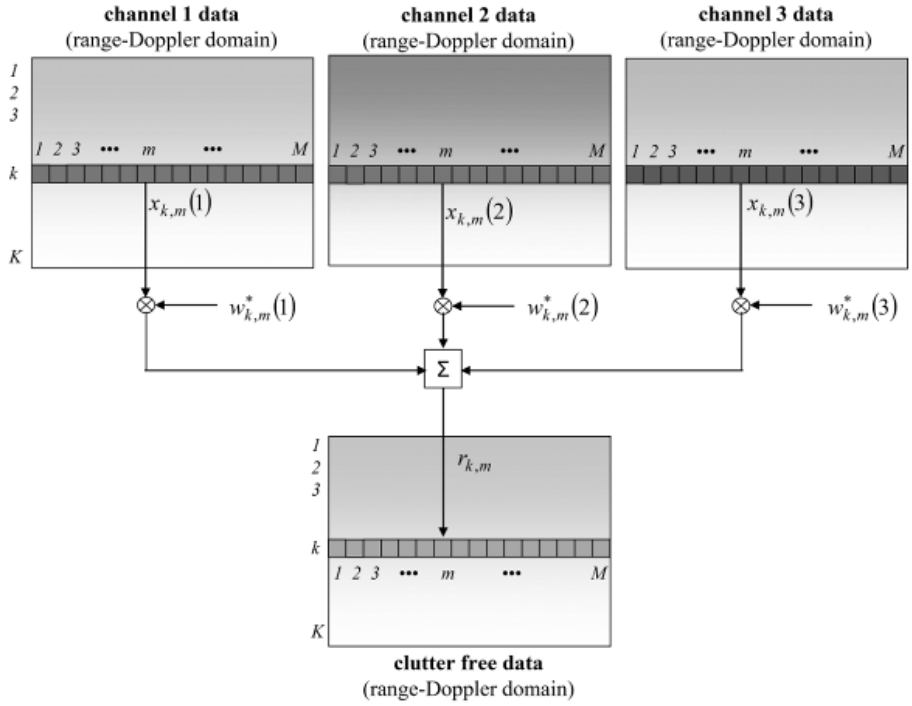

Fig. 11: Clutter cancellation in the Doppler frequency domain

Two important aspects have to be highlighted. Firstly, it is clear that the element-space post-Doppler STAP approach here considered performs a spatial-only adaptive nulling for each Doppler bin separately. This has the dual advantage to allow nearly optimum clutter cancellation performance (due to the Doppler bin decoupling for long CPIs) and also to drastically reduce the dimensions of the interference covariance matrix to be estimated and inverted, causing savings in computational burden. Secondly, the FFT in the azimuth domain required by the STAP technique is applied separately to the raw data acquired by each receiving channel. The azimuth FFT is also the first operation foreseen by the CSA, making feasible an efficient integration between the cancellation and the focusing steps.

Once the clutter cancellation is performed, the bank of focusing filters is applied to the resulting clutter free data thus giving rise to the Multi Channel - Bank of Chirp Scaling Algorithms, MC-BCSA, technique. The processing chain corresponding to the MC-BCSA technique is depicted in Fig. 12 for the sample case of a three channels (N=3) SAR system.

To show the effectiveness of the proposed MC-BCSA technique, a M-SAR datacube of an observed scene with several moving targets has been emulated in [18] starting from the same SAREX-92 image of the Tapajos rain forest already considered above. Assuming the stationary background (i.e. clutter) to be perfectly correlated in time, a multi-channel SAR dataset can be derived from the single-channel SAR dataset by resampling the signal in the slow-time domain. These three raw images have been added to thermal noise and to synthetic raw returns from several targets moving along roads A and B. In particular, a Clutter to Noise Ratio (CNRRAW) of 13 dB has been considered and, after focusing, an averaged CNRFOC of about 16 dB is experienced over the image. As far as the targets are concerned a Signal to Clutter Ratio (SCRRAW) of -28 dB (both measured on the single-channel raw data) has been chosen while targets velocities (and relative components in the cross/along-track directions) are those already used for the single-channel analysis, see Tab. 1. Both defocusing due to target motion and low SCRRAW value make difficult the detection of the movers.

The obtained M-SAR raw datacube is fed in input to the MC-BCSA processing chain in Fig. 12; the same M-SAR raw datacube has been also focused by means of traditional CSA with a preliminary STAP processing step done accordingly to the scheme in Fig. 11. In both cases the 3x3 interference covariance matrices have been estimated on the basis of P=6 secondary data samples.

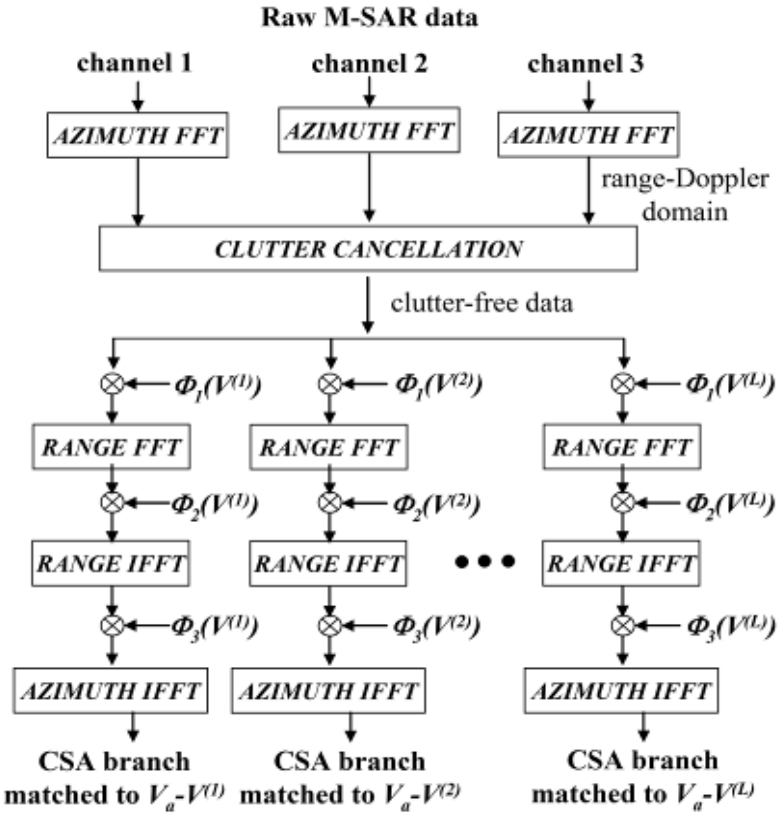

Fig. 12: Processing chain for MC-BCSA technique.

The effectiveness of the clutter cancellation has been verified by measuring the reduction of the clutter plus noise power in the focused image with respect to the "no STAP case" for which we have CNRFOC=16 dB. In particular, a reduction of the clutter plus noise power close to 13 dB has been observed. This value is approximately equal to the maximum theoretical reduction, achievable when the clutter level is lowered down to the noise level (clutter plus noise power reduction = CNRFOC – 3 dB).

Tab. 2: SCNRFOC values on focused images.

Target	NO STAP +	STAP +	MC-BCSA
1A	-0.48	14.16	16.20
2A	6.48	14.46	16.84
3A	6.43	15.93	16.41
1B	4.84	14.89	15.96
2B	3.71	13.84	14.67
3B	6.09	15.03	13.88

To analyze the detection performance, Tab. 2 reports the signal to clutter plus noise power ratio in image domain, SCNRFOC, evaluated for the different targets in the cases single channel & traditional focusing (no STAP - conventional CSA), multi channel & traditional focusing (STAP - conventional CSA) and multi channel & bank of CSA (MC-BCSA). Monte Carlo simulations with 100 trials have been used. The improvement of SCNRFOC moving from the single to the multi channel case can be appreciated by comparing the first two columns of Tab. 2. As it is clearly visible, the achieved SCNRFOC improvement is lower than the clutter plus noise power reduction. This is mainly due to a reduction of the power signal level due to cancellation especially for those targets with low velocities. In any case the resulting values of SCNRFOC guarantee a proper target detection capability. Nevertheless, these returns appear still defocused, making the bank of CSA needed for high-resolution imaging.

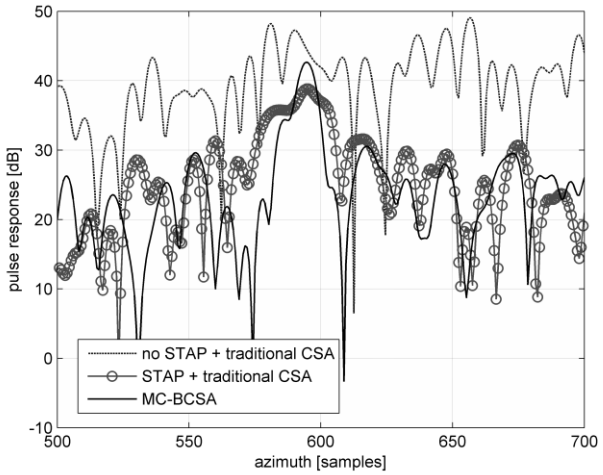

Fig. 13: Comparison of azimuth pulse responses for target 1A.

A further gain in the SCNRFOC value is obtained using the MC-BCSA technique, as shown in the third column of Tab. 2. To show the effectiveness of the integrated processing for high resolution imaging, we show in Fig. 13 a comparison among the azimuth pulse responses for no STAP - conventional CSA, STAP - conventional CSA and MC-BCSA, again for target 1A. In the MC-BCSA case, the target pulse response main-lobe becomes clearly visible against the reduced interference background.

The application of the integrated technique to the available sample scenario shows that both steps (i.e. clutter cancellation and bank of focusing filters) are necessary for low RCS target detection. The former allows to reduce the power level of stationary background making detectable the returns from moving targets, while the latter allows a correct imaging of the targets, recovering an acceptable azimuth resolution.

Finally, it intuitive to realize that the computational cost of the proposed technique can be lower than standard ATI (see Fig. 14), since this requires the application of a CSA for each channel, [23], [24].

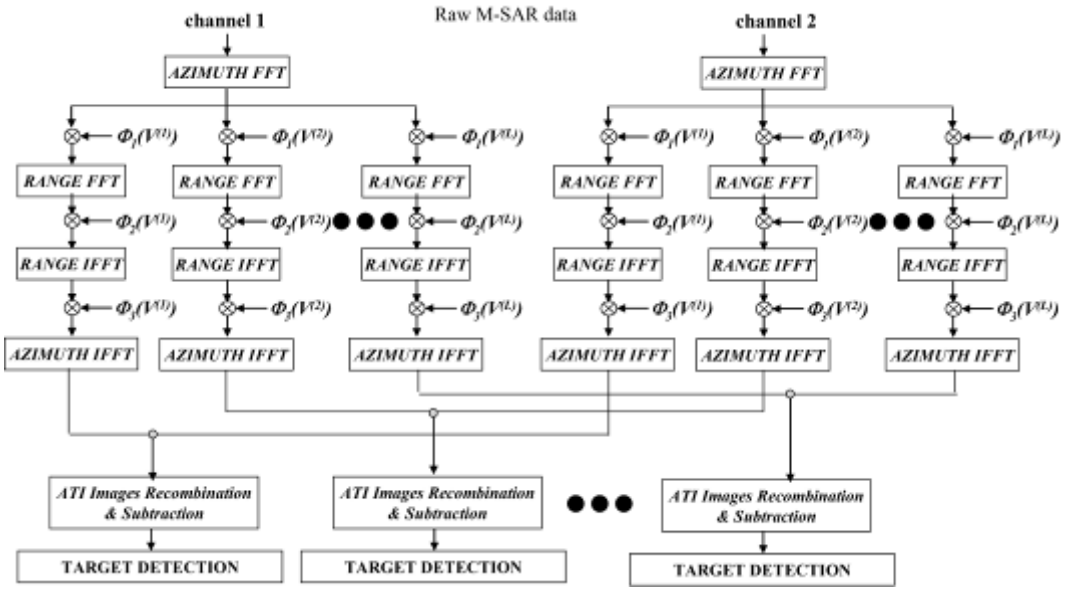

Fig. 14: ATI + bank of CSA

4.0 ALTERNATING SUB-APERTURE DETECTION

Among other elements, the performance of the STAP techniques strongly depends on the number of sub-arrays and on the spatial distance between their phase centers. The antenna size sets a constraint on the maximum separation between the extreme phase centers, which largely affects the width of the Space-Time filter notch. A larger antenna would provide a larger separation between extreme phase centers thus increasing the clutter resolution capability and enhancing slowly moving targets detection and DOA estimation performance. Unfortunately, both air- and space-borne applications set strong constraints on the size of the antenna array. A potential solution is to synthetically increase the maximum distance between phase centers by using only a sub-aperture to transmit the radar pulses, while alternating the transmitter (ALTX) between a leading (LS) and a trailing antenna sub-aperture (TS) from pulse to pulse, [25].

The idea behind ALTX is based on the spatial position of the two-way phase centers: Fig. 15a shows the case of standard transmit (STTX), namely transmitting with the whole antenna, and receiving with N=4 identical sub-apertures. The two-way phase centers are located mid-way between TX and RX phase centres, so that their maximum spacing is (1-1/N)·L/2, being L the antenna length. Fig. 15b and 15c show respectively the case of transmitting with LS only and TS only, and receiving with the same N sub-apertures. The position of the two-way phase centers moves with the TX. Therefore, the number of phase centers and their maximum distance can both be doubled by fast switching the TX alternatively between the two external antenna sub-apertures, at the expense of increasing the PRF. While changing the transmit antenna is not usual and subject to calibration problem, it is not uncommon in multipolarization systems to get quad-polarized data. Despite the doubled 'virtual' spatial channels are not simultaneously available, they can be aligned in time using an extension of the DPCA condition, which requires the radar PRF to be appropriately selected, in conjunction with the sequence of TX antenna switching (Fig. 16). This results in two-way phase centers that occupy the same location after a temporal interval of $\Delta T_{ALTX} = (1-1/N)\cdot L/vp = 2\Delta T_{STTX}$. However, using STAP clutter cancellation, phase center alignment is not required, so reasonable PRF values can be used.

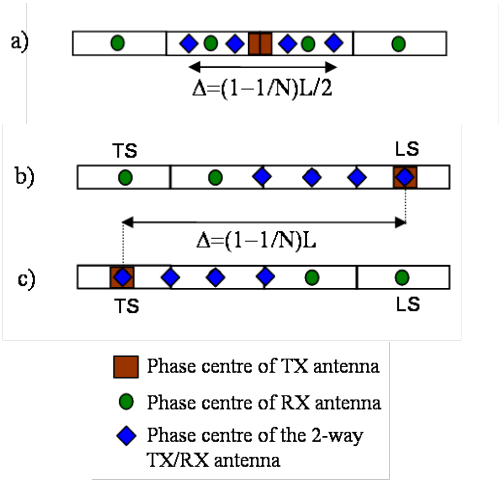

Fig. 15 – Sketch of the phase centers position with N=4 : (a) STTX, (b) LS TX, (c) TS TX.

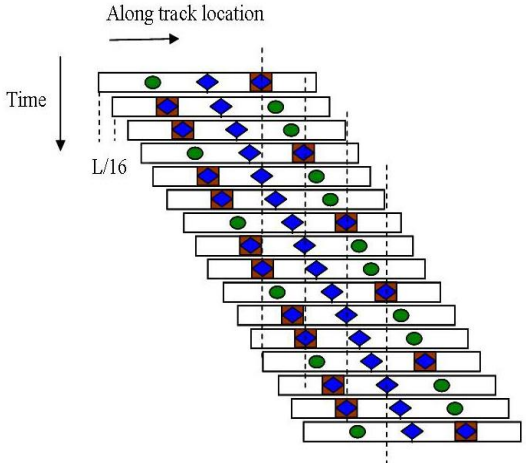

Fig.16 – Sketch of the phase centre motion for ALTX with a dual-channel antenna system.

To perform a fair comparison of STTX and ALTX modes, Fig. 2 shows the SCNRout assuming that in the two modes the same global energy is transmitted and the same duty cycle is used by the active elements. With this choice ALTX suffers a loss w.r.t STTX in the antenna directivity, since only a portion of the total antenna aperture is used in transmission (3dB when using alternatively a semi-aperture for transmission). The alternating sequence of TS and LS transmission should be appropriately selected to align phase centers, therefore we consider the case of PRF=8vp/L=853Hz:

A. Single receiving channel : with N=1 receiving channel and STTX (Fig. 2, symbol "×"), STAP cannot be performed and the clutter notch strongly depends on the antenna beam-width. By using ALTX (Fig. 2, symbol "o"), two fictitious channels are synthesized, which allows STAP. The SCNRout obtained with ALTX shows a 3dB loss w.r.t. STTX far away from the clutter notch. However the notch width is largely reduced and comparable to the notch obtained with STTX with N=2. Therefore, the detection capability of the very slowly moving targets can be improved using ALTX. In the case of N=1 an alternative approach is to use an alternating receiving channel (ALRX). This is obtained similarly to ALTX by using only a semi-aperture in reception. This might be preferable to ALTX in practice for the easier calibration expected and is also attractive for MSAR applications, [26].

B. Dual receiving channel: For N=2 receivers (Fig.2, symbol "□"), ALTX yields 3 synthetic channels with larger baseline, i.e. maximum temporal distance between aligned 2-way phase centers. The extra channel might be useful for DOA estimation, despite the detection loss w.r.t. STTX (symbol "∇").

In conclusion, ALTX allows to synthesize an equivalent distance between phase centers double than STTX, thus increasing the equivalent antenna, for a given physical array size, without requiring to increase the number of receiving channels. The better performance inside the notch can be paid in terms of transmitted power or PRF, especially outside the notch, and is convenient for specific applications.

5.0 BISTATIC MULTICHANNEL DETECTION

Several research activities are in progress on bistatic radar systems for both air-borne and space-borne applications. Bistatic radar offer several advantages over their monostatic counterparts, including the potential for enhanced target RCS, avoidance of eclipsing, reduced vulnerability to e.m. interferences, and

synergistic coherent operation with existing systems. Among their drawbacks bistatic radar must effectively cope with severe, spectrally diverse ground clutter returns due to the simultaneous transmitter (TX) and receiver (RX) motion which yields a non-stationary behaviour of the clutter spectra over bistatic range. Therefore, clutter suppression becomes a crucial issue for the detection of ground slowly-moving targets. STAP, first used for monostatic radar, is considered as an enabling technology also for bistatic MTI radars, [5], [27], [7]. However the non-stationary nature of bistatic ground clutter limits the implementation of STAP which relies on secondary data for covariance estimation. Fig. 17c-d shows the clutter Doppler-Angle spectral traces for Case I and Case II, sketched in Fig. 17a-b. In Case I the transmitter (TX) and receiver (RX) platforms are aligned on the same flight direction at equal heights (HR=HT), while in Case II the RX flies below the TX with a vertical baseline of B=6 Km. In both cases, λ=3cm (X band), M=12 pulses and Uniform Linear Arrays (ULA) are used composed of N=12 sensors. Results are shown at bistatic ranges RB=11km, RB=18km, RB=25km; spots indicate the position of the Spectral Centre (SC) in the Doppler-Angle plane due to TX and RX beam-pointing angles, [28]. Since clutter energy wanders in the Doppler-Angle domain as the bistatic range changes, STAP techniques require modifications. To make the linear filter adaptive, P echo vectors received from range cells adjacent to the CUT are considered available; they are called secondary data and are assumed to be target-free and to share the same covariance matrix of the cell under test. For the bistatic case, the covariance matrix is range dependent. The Improvement Factor (IF) as a function of the normalized Doppler frequency F is shown in Fig. 17e-f. In particular we refer to: (i) theoretical IF obtained by assuming known the covariance matrix Q0 of the CUT (OAP); (ii) asymptotical IF obtained by replacing Q0 with its asymptotic estimation QAS (the average over the covariance matrices of the secondary data Qk, k=1,..,P), with P=2NM=288 at RB=18 km and Clutter-to-Noise Ratios (CNR) of 21dB and 25dB for the two cases. The range-dependence leads to degraded STAP performance especially in Case I which has a severe spectral dispersion in the clutter main lobe area.

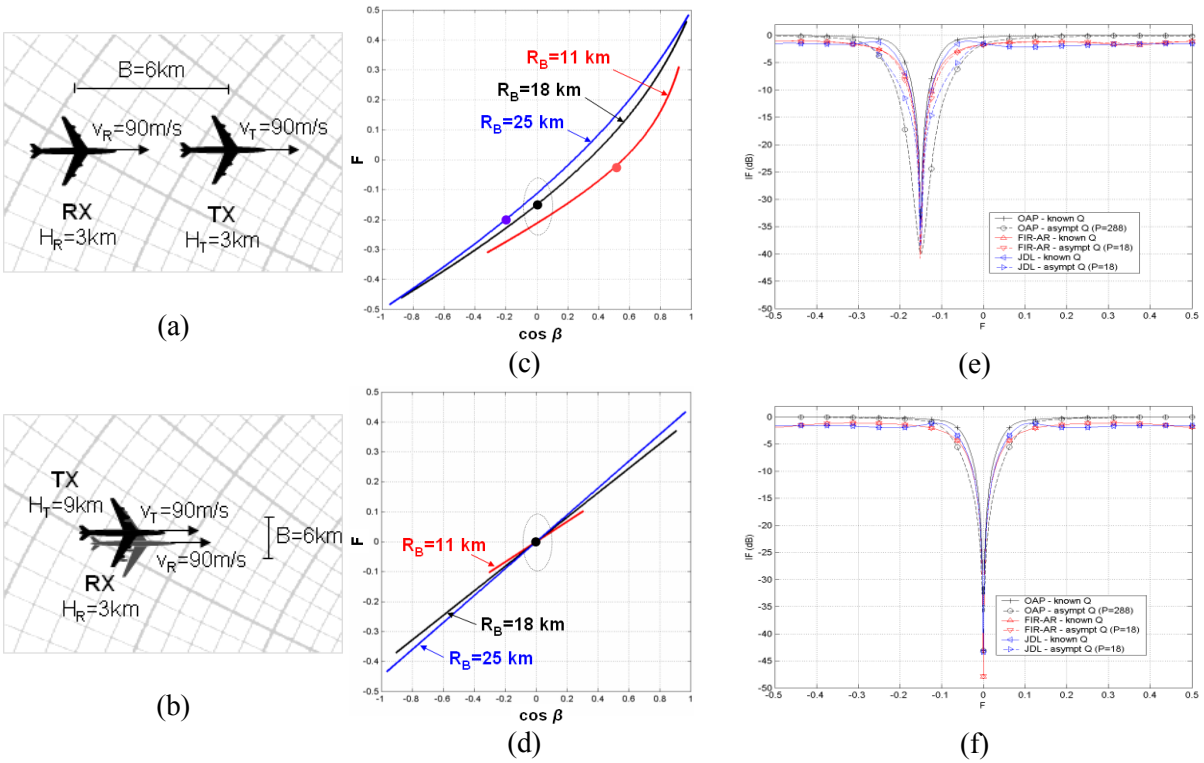

Fig. 17 – Study cases analysis: (a-b) sketch of the bistatic geometries of Case I e Case II; (c-d) clutter Doppler-Angle spectral traces for Case I and Case II.

A number of recent contributions have been reported, [28] - [40], where the clutter range-dependence problem is addressed and different approaches are proposed. Among them, reduced rank STAP techniques

have been considered aiming at minimizing the required sample support, [28] - [31]. This enables localized training in the range dimension and thus limited effects of clutter non-stationarity. However, some performance degradation may still occur for two reasons: limited or inappropriate adaptive degrees of freedom (d.o.f.) and, depending on the bistatic geometry, persistent clutter variability even over limited range extents. Fig. 17(e-f) show the results obtained with Joint Domain Localised (JDL) technique, [32], operating with K=L=3 spatial and temporal d.o.f. and an AR-based 2D FIR that uses L=3 taps with a non-adaptive beamforming to reduce the spatial d.o.f. from N=12 to K=3, [31]. Both operate with P=2KL=18 secondary data. The reduction of sample support yields a large improvement of asymptotical IF: in Case II, the performance loss is totally removed while, in Case I, a degradation still occurs due to residual clutter variability over the limited range. A different approach is the direct removal of the non-stationary characteristics from the bistatic data by applying ad hoc compensations, such as Doppler Warping (DW) which uses a deterministic complex taper to align clutter Doppler for specified cone angle (Fig. 18a), [33], [34], and the Angle-Doppler Compensation (ADC) which aligns peak angle-Doppler responses, or SC over range (Fig. 18b), [35], [36]. Advanced solutions are Higher Order Doppler Warping (HODW), which performs compensation over multiple cone angles, [37], and adaptive inverse transformations, [38]. However these techniques require the exact knowledge of the clutter Doppler-Angle spectral trajectory over range whose estimation can be limited by thermal noise especially in the clutter side lobes area. Moreover they can yield a high computational load.

A further compensation strategy was recently proposed in [39], [40], based on the idea of realigning the clutter spectral slopes after the SCs have been co-located. First perform an ADC to bring the spectral centers of the different range cells together. Then apply a transformation to realign the Doppler-Angle trajectory slopes around the clutter main lobe (Fig. 18c). To this purpose, the clutter Doppler-Angle spectral trajectory of each range cell is approximated by its First-Order (FO) Taylor expansion around the position of the SC and the slope compensation is obtained by performing a bin-dependent shifting which realigns the approximated trajectory with that of the CUT. Version 1 (v1) is obtained by shifting the trajectories over angular dimension, while version 2 (v2) is obtained by shifting over Doppler dimension. Since the slope variations are small around the clutter main lobe area for a given range cell, this approach exactly realigns the spectral trajectories of the secondary data thus further reducing the clutter dispersion with respect to previously approaches.

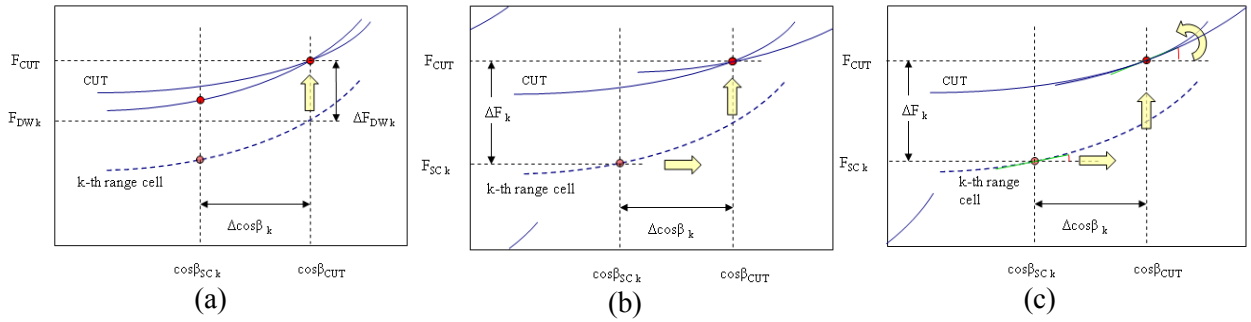

Fig. 18 -Sketch of the clutter dispersion compensation strategy for (a) DW; (b) ADC; (C) FO-ADC

The results obtained by applying the compensation strategies to the secondary data are reported in Fig. 19 (enlarged view of the notch area). As apparent, in Case I, ADC and DW yield a strong clutter dispersion reduction which implies a significant performance improvement in terms of asymptotical IF. In particular the ADC yields slightly better performance with respect to the DW. In contrast, in Case II, the considered compensation strategies are not effective since, for this bistatic geometry, the clutter spectral dispersion is essentially related to the Doppler-Angle trajectory slope variability over range that the considered approaches cannot compensate for. As apparent, the FO-ADC allows a further performance improvement in Case I yielding a slightly narrower notch with respect to DW and ADC (see Fig. 19a). The dispersion

compensation capability of FO-ADC is more evident in Case II, where the slope-based approach is the only one capable to partially recover the bistatic geometry-induced loss with a significant advantage over ADC and DW (see Fig. 19b).

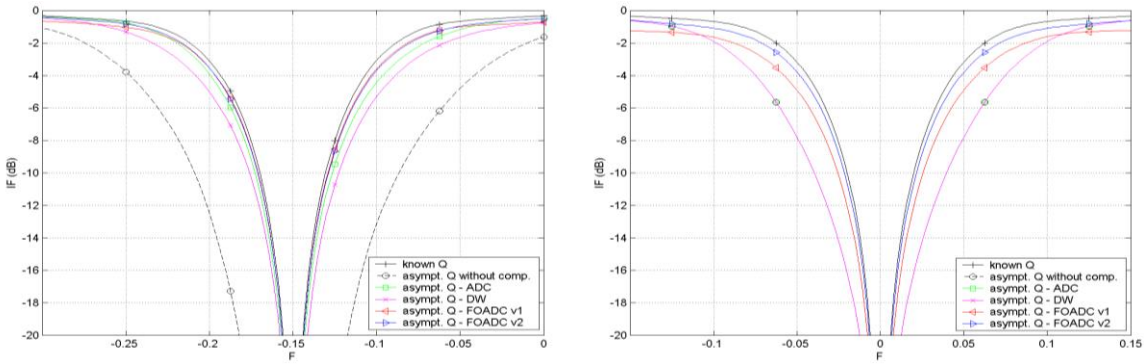

(a) (b)

Fig. 19 – IF vs Normalized Doppler F obtained for: (a) Case I; (b) Case II.

Fig. 20 shows the power spectra for Case I: the asymptotic estimation of the power spectrum obtained on the DW pre-processed secondary data (Fig. 20c) is significantly narrowed with respect to the case without compensation (Fig. 20b); however it shows a residual dispersion with respect to the ADC technique (Fig. 20d) which yields an asymptotic spectrum almost equal to that of the CUT (Fig. 20a). Fig. 21 shows the power spectra for Case II. As apparent the asymptotic estimation of the power spectrum on the uncompensated secondary data (Fig. 21b) is significantly broadened with respect to the theoretical spectrum of the CUT (Fig. 21a) despite the alignment of the SCs over range. The asymptotic estimation of the power spectra on the secondary data pre-processed using both versions of FO-ADC (Figs. 21c-d) is significantly narrowed with respect to the case without compensation. Notice that the latter coincides with the asymptotic spectra obtained using DW and ADC, since these techniques are not effective for this particular bistatic geometry. Moreover the FO-ADC asymptotic spectrum is almost identical to that of the CUT.

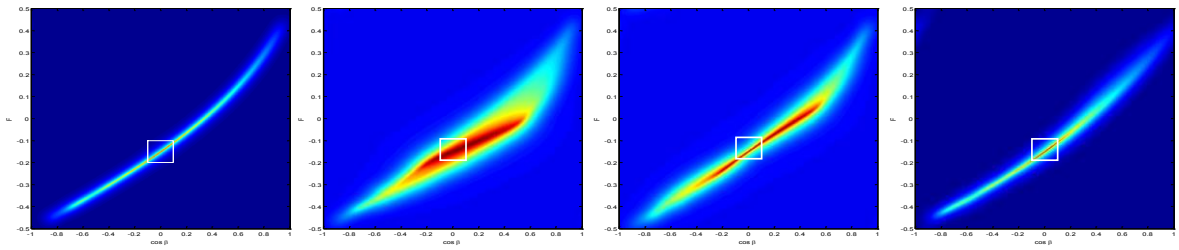

(a) (b) (c) (d)

Fig. 20 – MV power spectra for Case I: (a) CUT (known Q); (b) asymptotical estimation over secondary data without compensation; (c) DW; (d) ADC.

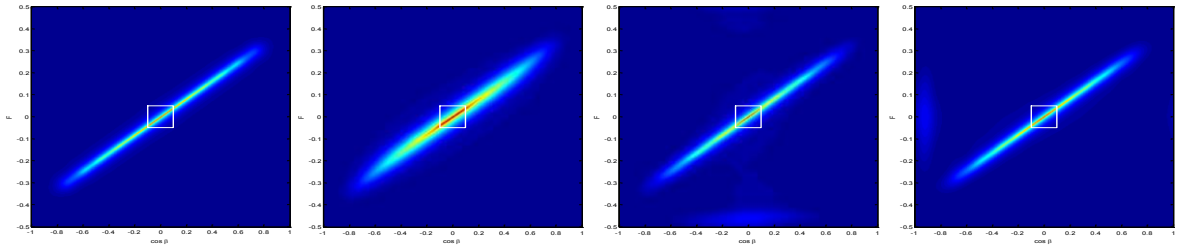

(a) (b) (c) (d)

Fig. 21 – MV power spectra for Case II: (a) CUT (known Q); (b) asymptotical estimation over secondary data without compensation (or applying DW/ADC); (c) FO-ADC v1; (d) FO-ADC v2.

The derived techniques make the use of the bistatic STAP feasible for the detection of low RCS, slowly moving targets with Multichannel SAR in the next generation of airborne and spaceborne surveillance systems.

6.0 ACKNOWLEDGEMENTS

The author gratefully acknowledges many useful conversations with Dr. Fabiola Colone, Dr. Debora Pastina and Dr. Diego Cristallini, as well as the many collaborations in the research activity carried out in the latest years on this subject.

7.0 REFERENCES

[1] Raney R. K., “Synthetic aperture imaging radar and moving target”, IEEE Trans. AES, 1971, 7, pp. 499-505.

[2] Pastina D., Battistello G., Aprile A., “Change detection based GMTI on single channel SAR images”, proc. of EuSAR 2008, vol. 3, pp. 85-88, 2-5 June 2008, Friedrichshafen, Germany.

[3] Kirscht, M.; "Detection and imaging of arbitrarily moving targets with single-channel SAR", IEE Proc.-RSN, Vol. 150, No. I, 2003, pp.7-11.

[4] Dias, J.; Marques, P.; "Multiple moving targets detection and trajectory parameters estimation using a single SAR sensor", IEEE Trans. AES, 39 (2003), pp. 604-624.

[5] R. Klemm, “Principle of Space-Time Adaptive Processing”, IEE, London, UK, (2002).

[6] A. Farina, P. Lombardo, “Space-time techniques for SAR”, chapter in "Applications of space-time processing", R. Klemm (Ed.), IEE Publisher, 2004.

[7] Melvin W.L., “A STAP Overview”, IEEE AES Magazine, Vol. 19, Jan. 2004, pp.19-35.

[8] P. Lombardo, "Echoes covariance modelling for SAR along-track interferometry", IEEE Int. Symposium IGARSS '96, Lincoln, Nebraska (USA), May 1996, pp. 347-349.

[9] C. Gierull, “Moving target detection with along-track SAR interferometry”, DREO TR 2002-000, 09 January 2002.

[10] B. Friedlander, B. Porat, “VSAR- a high resolution radar system for detection of moving targets”. IEE Proc. on Radar, Sonar and navigation, Vol. 144, No. 4, pp. 205-18, Aug 1997.

[11] P. Lombardo, "Optimum multichannel SAR detection of slowly moving targets in the presence of internal clutter motion", CIE-ICR '96, International Radar Conference Beijing, China, 8-11 Oct. 1996, pp. 321-325.

[12] R. Klemm, J. Ender ,”Two-dimensional Filters for Radar and Sonar Applications”, EUSIPCO’90, Sept 1990, Barcelona.

[13] S. Barbarossa, A. Farina, “Space-time-frequency processing of synthetic aperture radar signals”, IEEE Trans. on Aerospace and Electronic Systems, Vol. 30, No. 2, April 1994.

[14] P. Lombardo, “A Joint Domain Localized processor for SAR target detection”, European Conference on Synthetic Aperture Radar, EUSAR’98, Friedrichshafen (G), 25-27 May 1998.

[15] J. H. G. Ender, “Space time processing for multichannel synthetic aperture radar”, Electr. & Comm. Eng. Journal (ECEJ) Special Issue on STAP, Vol. 11, No.1, pp. 29-40, February 1999.

[16] Barbarossa S., “Detection and imaging of moving objects with synthetic aperture radar, Part 1”, IEE Proc.-F, 1992, 139, (1), pp. 79-88.

[17] Raney R. K., et alii, “Precision SAR processing using chirp scaling”, IEEE Trans. GRS, 1994, 32, (4), pp. 786-799.

[18] D. Cristallini, D. Pastina, F. Colone, P. Lombardo, “Efficient Detection and Imaging of Moving Targets in SAR Images Based on Chirp Scaling”, IEEE Transactions on Geoscience and Remote Sensing (GRS), Vol. 51, N. 4, Part 2, April 2013, pp. 2403- 2416.

[19] Hoekman, D.H.; van der Sanden, J.J.; Bijker, W.; , "The AIRSAR-93 and SAREX-92 campaigns in Guyana and Colombia," Proc of IGARSS '94. Surface and Atmospheric Remote Sensing: Technologies, Data Analysis and Interpretation., International , vol.2, no., pp. 1051- 1053 vol.2, 8-12 Aug. 1994.

[20] Oliver, C.J.; , "Rain forest classification based on SAR texture," Geoscience and Remote Sensing, IEEE Transactions on , vol.38, no.2, pp.1095-1104, Mar 2000.

[21] Wei-Biao Wu, “Fourier Transforms of Stationary Processes”, Proc. of the American Mathematical Society, vol. 133, no. 1, pp. 285-293.

[22] Ward J., “Space-Time Adaptive Processing for Airborne Radar”, Technical Report 1015, MIT Lincoln Laboratory, Lexington, MA, USA, 1994 (available: http://handle.dtic.mil/100.2/ADA293032).

[23] Gierull C. H., “Statistical analysis of multi-look SAR interferograms for CFAR detection of ground moving targets”, IEEE Trans. GRS, 2004, 42, (4), pp. 691-701.

[24] Budillon A., Pascazio V., Schirinzi G., “Multichannel Along-Track Interferometric SAR Systems: Moving Targets Detection and Velocity Estimation”, Int. Journal of Navigation and Observation, vol. 2008, pp. 1-16.

[25] P. Lombardo, F. Colone, “An Alternating Transmit Approach for STAP with Short Antenna Arrays”, Proc. of the IEEE Radar Conf., 26-29 April 2004, Philadelphia, pp. 420-425.

[26] P. Lombardo, F. Colone, D. Pastina, “Monitoring and Surveillance Potentialities obtained by splitting the antenna of the COSMO-SkyMed SAR into multiple sub-apertures”, IEE Proc. of Radar Sonar and Navigation, Vol. 153, N. 2, April 2006, pp. 104-116.

[27] Klemm R., “Comparison between Monostatic and Bistatic Antenna Configurations for STAP”, Trans. of IEEE on Aerospace and Electronic Systems, Vol. 36, N. 2, April 2000.

[28] Himed B., Michels J.H., Zhang Y., (2001), “Bistatic STAP Performance Analysis in Radar Applications”, Proc. of IEEE Conference on Radar 2001, pp. 198-203.

[29] Melvin W.L., Callahan M.J, Wicks M.C., (2000), “Adaptive Clutter Cancellation in Bistatic Radar”, Conference on Signals, Systems and Computers 2000, Vol.: 2, pp.1125-1130.

[30] F. Colone, M. Labriola, F. Poli, P. Lombardo, "A Pre-Doppler Approach for Reduced Loss Bistatic STAP", 2006 CIE International Conference in Radar, Shanghai (China), Oct. 2006.

[31] P. Lombardo, F. Colone, "Non-linear and Adaptive two-dimensional FIR filters for STAP: theory and experimental results", chapter in "Applications of space-time processing", R. Klemm (Ed.), IEE Publ., 2004.

[32] H. Wang, L. Cai, (1994): 'On adaptive spatial-temporal processing for airborne surveillance radar systems', IEEE Trans. on AES, Vol. 30, No. 3, July 1994, pp. 660-670.

[33] Borsari G.K., (1998), "Mitigating Effects on STAP Processing Caused by an Inclined Array", Proc. of the 1998 IEEE Radar Conference, RADARCON 98., 11-14 May, pp. 135-140.

[34] Kogon S M., Zatman M. A., (2000), "Bistatic STAP for Airborne Radar System", Proc. IEEE SAM, Lexington, MA.

[35] Himed B., (2003), "Effect of Bistatic Clutter Dispersion on STAP system", IEE Proceedings Radar, Sonar and Navigation, Vol. 150, Issue 1, Feb. 2003.

[36] Melvin W.L., Himed B., Davis M.E., (2003), "Doubly Adaptive Bistatic Clutter Filtering", Proc. of IEEE Conference on Radar 2003, pp. 171-178.

[37] Pearson F., Borsari G., (2001), "Simulation Analysis of Adaptive Interference Suppression for Bistatic Surveillance Radars", Proc. of ASAP Symposium, Lexington, MA, Mar. 13, 2001.

[38] Lapierre F.D.; Verly J.G.; Van Droogenbroeck M., "New Solutions to the Problem of Range Dependence in Bistatic STAP Radars", Proc. of 2003 IEEE Conf. on Radar, pp. 452-459.

[39] F. Colone, M. Fornari, P. Lombardo, "A spectral slope-based approach for mitigating bistatic STAP clutter dispersion", submitted to the IEEE Radar Conference 2007.

[40] F. Colone, "A spectral slope-based approach for mitigating bistatic STAP clutter dispersion", IET Radar Sonar and Navigation, Volume 5, Issue 5, June 2011, pp. 593-603.